AIP | Applied Physics Letters

The interplay between strain and size effects on the thermal conductance of grain boundaries in graphene

Shengjie Tang and Yashashree Kulkarni

Citation: Appl. Phys. Lett. **103**, 213113 (2013); doi: 10.1063/1.4833636
View online: http://dx.doi.org/10.1063/1.4833636
View Table of Contents: http://apl.aip.org/resource/1/APPLAB/v103/i21
Published by the AIP Publishing LLC.

The interplay between strain and size effects on the thermal conductance of grain boundaries in graphene

Shengjie Tang and Yashashree Kulkarni[a)]
Department of Mechanical Engineering, University of Houston, Houston, Texas 77204, USA

(Received 12 August 2013; accepted 11 November 2013; published online 21 November 2013)

The effect of strain on the thermal transport across grain boundaries in graphene is investigated using molecular dynamics simulations. The thermal boundary conductance is found to decrease significantly under biaxial tension as expected. In contrast, under biaxial compression, the thermal boundary conductance is strongly affected by the dimensions of the graphene monolayer, increasing with strain for specimen with length-to-width ratio of less than 20 and being insensitive to strain for length-to-width ratio above 20. This rather unexpected size-dependence under biaxial compression is found to be a result of geometric instabilities. © *2013 AIP Publishing LLC*. [http://dx.doi.org/10.1063/1.4833636]

Graphene, a two-dimensional material consisting of a single layer of carbon atoms, possesses exceptional electronic, optical, thermal, and mechanical properties, which make it an outstanding material for next-generation energy, electronics, and thermal management applications.[1–4] Turning this promise into reality requires the synthesis of large-area single crystal graphene sheets which still poses a major challenge. Despite a strong drive towards developing novel methods for growing super-sized single-crystal domains,[5] recent advances in large-scale production of monolayer graphene sheets via chemical vapor deposition typically result in polycrystalline graphene[6–8] whose properties can be drastically affected by the presence of grain boundaries. Several experimental and atomistic studies spanning the past decade have demonstrated the excellent thermal conductivity of carbon nanotubes and single crystal graphene.[9–13] Atomistic investigation of the thermal transport across grain boundaries and defects in graphene has been relatively recent.[14–19] Several molecular dynamics studies have also investigated the role of strain in manipulating the thermal properties of graphene and carbon nanotubes for potential applications in adaptive thermal management and thermoelectrics with tunable properties.[20–23] However, the influence of strain on the thermal transport properties of grain boundaries has remained relatively unaddressed. Recent studies have probed the effect of strain on the interface between a carbon nanotube pillar standing on a graphene sheet and effect of tensile strain on the interfacial thermal resistance of isotope doped graphene.[24,25] In this Letter, we report our investigation of the influence of tensile and compressive strains on the thermal transport across grain boundaries in graphene.

The thermal boundary conductance, also known as the Kapitza conductance,[26] of the grain boundary is calculated using reverse nonequilibrium molecular dynamics (RNEMD) simulations. Following the Muller-Plathe approach,[27,28] we first define two "cold" slabs, located at the ends of the simulation cell, and a "hot" slab, located in the middle, as shown in Figure 1. The heat flux is introduced by continuously transferring energy from a "cold" slab to the "hot" slab which is accomplished by exchanging the velocities of the hottest atom in the cold slab and the coldest atom in the hot slab. The resulting heat flux, denoted by J, is given by the sum of all energy transfers per unit time per unit area[14,20]

$$J = \frac{1}{2tA}\sum_{N_{transfer}} \frac{m}{2}(v_{hot}^2 - v_{cold}^2) \ , \tag{1}$$

where t is the total simulation time, A is the cross-sectional area perpendicular to the direction of heat flow, m is the mass of the atoms, v_{hot} and v_{cold} are the velocities of the hottest atom of the cold region and the coldest atom of the hot region, respectively, and $N_{transfer}$ denotes the number of exchanges performed during time t.

After steady state is reached, there exists a discontinuity in the temperature profile at the interface which we denote by ΔT (Figure 1). The jump gives a measure of the boundary conductance (Kapitza conductance) G_κ of the grain boundary through the relation[29]

$$G_\kappa = -\frac{J}{\Delta T} \ . \tag{2}$$

Our simulations were performed on zigzag-oriented graphene with a rectangular cell geometry and two grain boundaries located along the x-direction as shown in Figure 1. Here, we considered a symmetric tilt boundary with a misorientation angle of 21.7°. Its structure consists of a single hexagonal ring separating the periodic 5–7 defects.[14,15,30]

Periodic boundary conditions were employed both along the direction of the heat flow (x-direction) and perpendicular to it (y-direction). The thickness of the monolayer was taken as 0.34 nm. The length of the simulation cell was varied from 25 to 100 nm, while the width was fixed at 5.21 nm. Cao and Qu[15] found that doubling the width of the graphene specimen introduced no appreciable effect on their Kapitza conductance results once the width was larger than 5 nm. The atomic interactions were expressed using a modified version of the Tersoff potential developed by Lindsay and Broido.[31] The potential has been shown to have a good agreement between the values of the acoustic-phonon

[a)]Electronic mail: ykulkarni@uh.edu

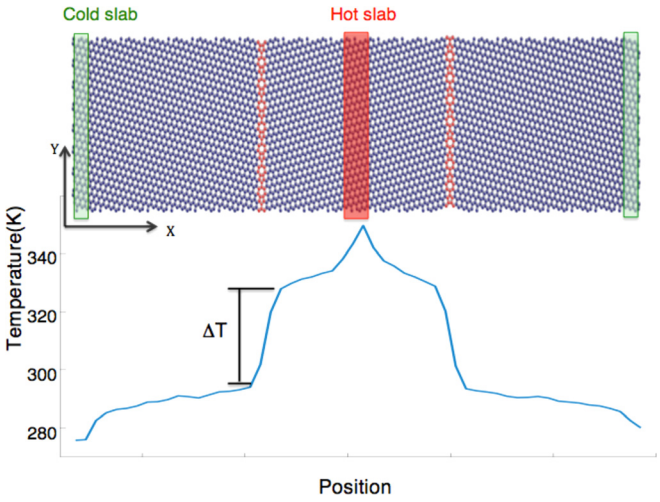

FIG. 1. Graphene monolayer in zigzag orientation (blue atoms) with two grain boundaries (red atoms). The grain boundary misorientation angle is 21.7°. The cold slabs on either end of the simulation cell and the hot slab in the middle are shown using green and red colors, respectively. The bottom figure shows a typical temperature profile with a distinct temperature discontinuity at the two grain boundaries.

velocities and experimental data in single-walled carbon nanotubes and graphene.[18,32] All simulations were performed using LAMMPS.[33] The system was first relaxed by running an NPT simulation for 100 ps at a background temperature of 300 K. The time step was set at 1 fs. A biaxial strain was then applied by elongating or compressing the specimen along both x and y directions at a strain rate of $10^9 s^{-1}$. To this end, an incremental strain of 0.001 was applied in both directions at every 1000 time steps under an NVT ensemble for a total time period of 400 ps. Finally, RNEMD simulations were performed, under NVE conditions, on different biaxially strained structures at room temperature. The simulation cell was divided into slabs of 5 Å width. To obtain the temperature profile, the system was allowed to evolve for 31 ns to reach steady state and then the temperature gradient through the structure was obtained by averaging over 3 ns.

Our simulations were performed using the *fix thermal/conductivity* command in LAMMPS in which the exchange of velocities is performed every N steps. In order to study the sensitivity of our results to the parameter N, we simulated the thermal conductance of the grain boundary at 300 K with different values of N ranging from 20 to 200 time steps. We found that the thermal conductance was not sensitive to the relaxation time which was also observed by Jiang *et al.*[34] in their recent thermal conductivity calculations on MoS_2. We chose $N = 40$ time steps, that is, a relaxation time of 0.04 ps in all our simulations.

To validate our simulation code, we calculated the thermal conductivity of single crystal graphene. We obtained the thermal conductivity of cells with periodic lengths of 25, 50, 100 nm as 261, 522, and 824 W/(m K), respectively. Using the phonon mean free path in graphene, we estimated the size-independent thermal conductivity to be 2778 W/(m K), which is in agreement with other atomistic simulation results.[18] The grain boundary energy for the 21.7° symmetric tilt boundary was computed to be about 2.2–2.7 eV/nm which was close to that obtained by Yazyev and Louie.[35] Furthermore, the Kapitza conductance of this grain boundary in a 100 nm specimen similar to that used by Bagri *et al.*[14] was found to be 15.34 GW/m^2K, which is in excellent agreement with their results.

Figure 2 shows the variation of the Kapitza conductance of the grain boundary with strain. We first note that the Kapitza conductance for unstrained graphene increases with specimen length. We performed calculations for larger specimen and found it to converge at about 300 nm which agrees with the findings of Cao and Qu.[15] Since the trends for the strain dependence observed in our simulations remain similar for larger specimen, we focus our subsequent discussion on specimen lengths varying from 25 to 100 nm. Under tension, the Kapitza conductance is shown to decrease significantly with increasing strain with similar response for specimen of different lengths. For a 3% tensile strain, we observe over 20% decrease in the Kapitza conductance. This reduction, also displayed by the thermal conductivity, is attributed to softening of the phonon modes with increasing lattice spacing under tensile strain. This is also confirmed by Pei *et al.*[25] who observe a reduction in high frequencies in the phonon spectrum of the interfacial atoms under tension and a concomitant decrease in the boundary conductance. Under biaxial compression, however, the Kapitza conductance exhibits a much more dramatic size-dependence both qualitatively and quantitatively, owing to the out-of-plane deformation modes. The bottom inset in Figure 2 shows the buckled structure of the 24 nm graphene specimen under biaxial compression. For the 24 nm long specimen, the Kapitza conductance increases with increasing strain and we obtain over 30% increase at 3% compressive strain. On the other hand, the Kapitza conductance of the 100 nm specimen remains unchanged even up to 15% strain. Biaxial compression tests on specimen up to 300 nm in length also show no effect of strain on the Kapitza conductance. This trend is in surprising contrast to the variation of the thermal conductivity which is known to decrease with biaxial compressive

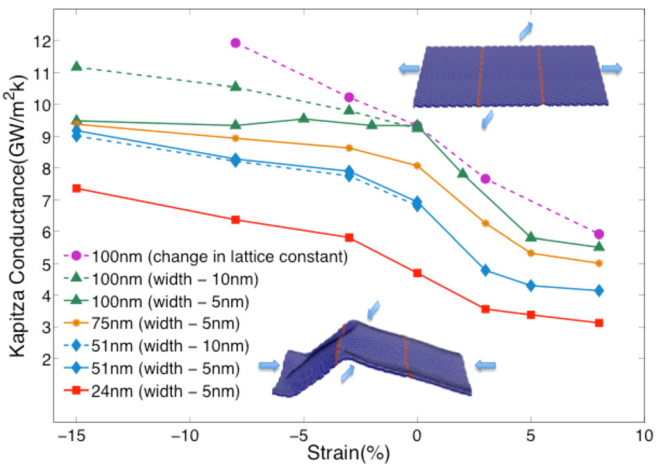

FIG. 2. Variation of the Kapitza conductance of the 21.7° symmetric tilt boundary with strain. The different curves were obtained for specimen lengths varying from 24 nm to 100 nm. Insets: Structure of the 24 nm specimen subjected to compressive (bottom), and tensile (top) biaxial strain of 3% along X and Y directions. For comparison, the dashed line with circles shows the variation of the Kapitza conductance when the strain is applied as a change in the lattice constant which keeps the monolayer flat in compression.

strain. Classical lattice thermal transport theory predicts the thermal conductivity as

$$\kappa = \sum_m C v_m l, \tag{3}$$

where C, v_m, and l are the specific heat, group velocity, and mean free path of the phonon mode m, respectively. As observed in several prior works on graphene and carbon nanotubes,[20–22] the scattering of the phonon waves at the irregular interfaces created due to buckling reduces the effective mean free path of the phonons which in turn reduces the thermal conductivity. To further investigate the role of buckling on the thermal boundary conductance, we also plotted its variation with the biaxial strain applied as a change in the lattice parameter to keep the graphene sheet flat during compression. The results are shown by the dashed line with circles in Figure 2. Analogous to the expected response under tension discussed earlier, the monotonic (almost linear) increase in the Kapitza conductance with decreasing lattice spacing is attributed to the stiffening of the phonon modes. Thus, it is evident that the geometric instabilities under compression have a complex effect on the phonons and hence on the Kapitza conductance.

The insensitivity of the Kapitza conductance to compressive strain begins to appear in our specimen with length 100 nm and longer or with length-to-width ratio of about 20. To probe this apparent size-effect, we repeated our simulation for the 100 nm specimen by doubling the width, that is, by changing the aspect ratio to about 10. The result, indicated by the dashed green line in Figure 2, shows an increasing Kapitza conductance with strain, similar to that observed for the smaller specimen. We also performed an additional simulation for the 50 nm specimen with 10 nm width. There is negligible difference between the curves for the 10 nm and the 5 nm cases both of which have length-to-width ratio less than 20 and have different widths. Taken together, these simulations reveal that the length-to-width ratio, and not the width, of the specimen is a determining factor in the strain governed Kaptiza conductance of graphene grain boundaries. Our simulations show that the Kapitza conductance of graphene sheets with length-to-width ratio of greater than 20 exhibits strain insensitivity under biaxial compression, which is possibly associated with a transition in the buckling modes. To investigate this further, we also computed the conductance of the same specimen with width of 5.21 nm and lengths varying from 25 to 100 nm subjected to uniaxial compression applied along the length of the specimen. As shown in Figure 3, the Kapitza conductance is found to remain insensitive to compressive strain for all specimen lengths. In agreement with our results, Wei *et al.*[22] also found the thermal conductivity of single crystal graphene to be unaffected by uniaxial strain. Taken together, our results confirm that above the critical length-to-width ratio of about 20, the buckling deformation under biaxial compression approaches that observed under uniaxial compression. This is also qualitatively illustrated by the deformed structures of the 100 nm specimen under biaxial and uniaxial specimen shown in Figure 4. The wider specimen with length-to-width-ratio of 10 shows a distinctly more crumpled structure

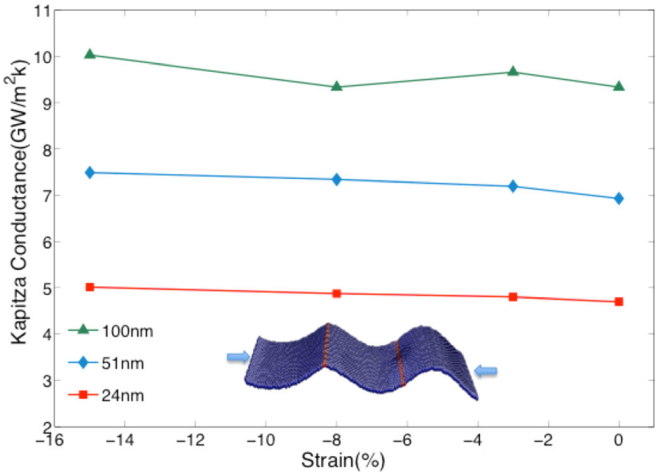

FIG. 3. Variation of the Kapitza conductance of the 21.7° symmetric tilt boundary in a graphene monolayer of different lengths under uniaxial compression. Inset: Deformed structure of the 24 nm specimen subjected to 3% uniaxial compressive strain.

under biaxial compression leading to more phonon scattering, whereas the slender specimen with length-to-width-ratio of 20 shows a wavy, wrinkled structure similar to that observed under uniaxial compression.

Under uniaxial compressive strain, the out-of-plane bending deformation of the graphene sheet releases the in-plane compressive strain. Thus, the phonon spectrum remains unaffected which in turn leads to constant thermal conductivity and Kapitza conductance. In contrast, the buckles or irregular surfaces generated under biaxial compression are regions of high localized strains. According to the acoustic mismatch model for thermal transport across interfaces, the Kapitza conductance is given by[29,36]

$$G_\kappa = \frac{1}{\Omega}\sum_m \omega_m v_m \frac{\partial n(\omega_m, T)}{\partial T}\alpha_m, \tag{4}$$

where Ω is the system volume, ω_m is the frequency for mode m, n is the Bose-Einstein distribution function, and α is the energy transmission coefficient for the interface. Comparing Eqs. (3) and (4), we note that apart from the common dependence on the phonon frequency (and the group velocity), the thermal conductivity depends on the phonon mean free path whereas the Kapitza conductance depends on the interfacial transmission coefficient. We believe that it is this difference that gives rise to the contrasting response of the

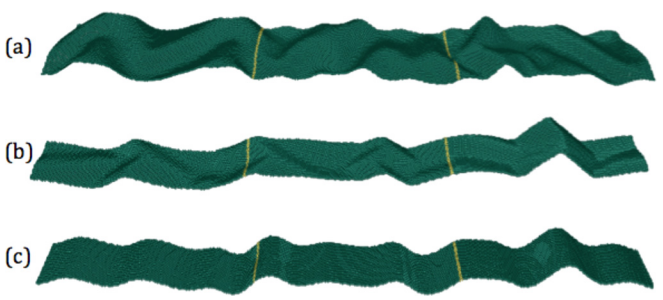

FIG. 4. Deformed structure of the 100 nm graphene specimen at 3% strain for three different cases: (a) Biaxial compression of the 10 nm wide specimen; (b) biaxial compression of the 5 nm wide specimen; and (c) uniaxial compression of the 5 nm wide specimen.

thermal conductivity and the Kapitza conductance under biaxial compression. As mentioned earlier, the buckles may be regarded as localized defects that scatter the phonons and reduce their mean free path leading to a decrease in the thermal conductivity. However, the effect of the defect scattering on the transmission coefficient of an interface is not so evident, especially under compression accompanied by geometric instabilities, and has been relatively unaddressed in literature. Recently, Jiang *et al.*[23] computed the transmission function for single-walled carbon nanotubes based on the non-equilibrium Green's function approach and showed that both tensile and compressive strains reduce the thermal conductance by filtering out certain low and high frequency phonons. Some theoretical and experimental studies on a solid-liquid interface in the past have indeed shown an enhancement in the transmission coefficient (and hence the Kapitza conductance) of the interface due to phonon scattering at defects such as random strain fields, dislocations, or point defects in its close vicinity.[37,38] Based on the theory of electron tunneling in quantum mechanics, the studies suggest that the scattering of phonons at the nearby defects or defects in the interface can change the angle of the incident phonons such that it enables acoustic coupling, or in other words, provides pathways for an increased transmission of phonons across the interface. In our biaxial compression simulations, we do find that some of the buckled regions usually cross the grain boundaries or are located very close to them.

In summary, we have performed non-equilibrium molecular dynamics simulations to illustrate an intriguing effect of strain on the Kapitza conductance of grain boundaries in graphene. Our results show that the Kapitza conductance decreases with tension, as expected, due to the softening of the phonons incident on the grain boundary. However, an interesting interplay between the size and strain dependence is observed under biaxial compression. We also studied the effect of temperature by comparing our results for 300 K and 600 K. We found that the Kapitza conductance of the unstrained graphene was in agreement with existing literature,[15,23] exhibiting an increase in conductance with increasing temperature. Moreover, the observations for the coupled strain and size dependence under biaxial tension and compression remain the same. Since the effect of strain seems to be dominated by the deformed shape and the aspect ratio of the graphene monolayer, we expect other tilt boundaries in graphene to also show similar behavior. Thus, our study suggests that the thermal boundary conductance should become size-independent for grain sizes larger than about 300 nm and should also become insensitive to compressive strain for specimen with length-to-width ratio of greater than about 20. These predictions could be useful for designing graphene-based materials for adaptable thermal management and thermoelectric applications. Further experimental and theoretical studies are needed to fully elucidate the mechanism for the increase in Kapitza conductance coupled with a decrease in the effective thermal conductivity observed for some specimen under biaxial compression. It would also be insightful to study the role of other defects such as vacancies and voids in governing the thermal conductance of the boundaries and the overall thermal conductivity of polycrystalline graphene.

The authors would like to acknowledge the support of the U.S. National Science Foundation under Grant No. CMMI-1129041 and the Defense Advanced Research Projects Agency under Grant No. N66001-10-1-4033. The simulations were performed partly on the supercomputing facility hosted by the Research Computing Center at University of Houston.

[1]A. K. Geim and K. S. Novoselov, Nature Mater. **6**, 183 (2007).
[2]A. F. Young and P. Kim, Annu. Rev. Condens. Matter Phys. **2**, 101 (2011).
[3]M. Pumera, Energy Environ. Sci. **4**, 668 (2011).
[4]A. A. Balandin, Nature Mater. **10**, 569 (2011).
[5]P. M. Ajayan and B. I. Yakobson, Nature. Mater. **10**, 415 (2011).
[6]K. S. Kim, Y. Zhao, H. Jang, S. Y. Lee, J. M. Kim, J. H. Ahn, P. Kim, J. Y. Choi, and B. H. Hong, Nature **457**, 706 (2009).
[7]X. S. Li, W. W. Cai, J. H. An, S. Kim, J. Nah, D. X. Yang, R. Piner, A. Velamakanni, I. Jung, E. Tutuc, S. K. Banerjee, L. Colombo, and R. S. Ruoff, Science **324**, 1312 (2009).
[8]G.-H. Lee, R. C. Cooper, S. J. An, S. Lee, A. van der Zande, N. Petrone, A. G. Hammerberg, C. Lee, B. Crawford, W. Oliver, J. W. Kysar, and J. Hone, Science **340**, 1073 (2013).
[9]S. Berber, Y. K. Kwon, and D. Tomanek, Phys. Rev. Lett. **84**, 4613 (2000).
[10]P. Kim, L. Shi, A. Majumdar, and P. L. McEuen, Phys. Rev. Lett. **87**, 215502 (2001).
[11]E. Pop, D. Mann, Q. Wang, K. Goodson, and H. Dai, Nano Lett. **6**, 96 (2006).
[12]A. A. Balandin, S. Ghosh, W. Bao, I. Calizo, D. Teweldebrhan, F. Miao, and C. N. Lau, Nano Lett. **8**(3), 902–907 (2008).
[13]Z. Guo, D. Zhang, and X.-G. Gong, Appl. Phys. Lett. **95**, 163103 (2009).
[14]A. Bagri, S.-P. Kim, R. S. Ruoff, and V. B. Shenoy, Nano Lett. **11**, 3917 (2011).
[15]A. Cao and J. Qu, J. Appl. Phys. **111**, 053529 (2012).
[16]Y. Lu and J. Guo, Appl. Phys. Lett. **101**, 043112 (2012).
[17]P. Wang, B. Gong, Q. Feng, and H.-T. Wang, Acta Mech. Sin. **28**, 1528 (2012).
[18]J. Hasking, A. Kinaci, C. Sevik, H. Sevincli, G. Cuniberti, and T. Cagin, ACS Nano **5**, 3779 (2011).
[19]A. Y. Serov, Z.-Y. Ong, and E. Pop, Appl. Phys. Lett. **102**, 033104 (2013).
[20]Z. P. Xu and M. J. Buehler, Nanotechnology **20**, 185701 (2009).
[21]X. Li, K. Maute, M. L. Dunn, and R. Yang, Phys. Rev. B **81**, 245318 (2010).
[22]N. Wei, L. Xu, H. Q. Wang, and J. C. Zheng, Nanotechnology **22**, 105705 (2011).
[23]J.-W. Jiang, J.-S. Wang, and B. Li, J. Appl. Phys. **109**, 014326 (2011).
[24]G. C. Loh, E. H. T. Teo, and B. K. Tay, J. Appl. Phys. **111**, 013515 (2012).
[25]Q.-X. Pei, Y.-W. Zhang, Z.-D. Sha, and V. B. Shenoy, Appl. Phys. Lett. **100**, 101901 (2012).
[26]P. L. Kapitza, *Collected Papers of P. L. Kapitza* (Pergamon Press, Oxford, 1967).
[27]F. Muller-Plathe, J. Chem. Phys. **106**, 6082 (1997).
[28]F. Muller-Plathe and D. Reith, Comput. Theor. Polym. Sci. **9**, 203 (1999).
[29]P. K. Schelling, S. R. Phillpot, and P. Keblinski, J. Appl. Phys. **95**, 6082 (2004).
[30]T. H. Liu, G. Gajewski, C. W. Pao, and C. C. Chang, Carbon **49**, 2306 (2011).
[31]L. Lindsay and D. Broido, Phys. Rev. B **81**, 205441 (2010).
[32]L. Lindsay, D. Broido, and N. Mingo, Phys. Rev. B **82**, 161402 (2010).
[33]S. Plimpton, J. Comput. Phys. **117**, 1 (1995).
[34]J.-W. Jiang, H. S. Park, and T. Rabczuk, J. Appl. Phys. **114**, 064307 (2013).
[35]O. V. Yazyev and S. G. Louie, Phys. Rev. B **81**, 195420 (2010).
[36]E. S. Landry and A. J. H. McGaughey, Phys. Rev. B **80**, 165304 (2009).
[37]F. W. Sheard and G. A. Toombs, J. Phys. Colloq. **33**, C4-61 (1972).
[38]W. L. Johnson and A. C. Anderson, Phys. Lett. A **37**, 101 (1971).